

Journal of Materials Chemistry A

Accepted Manuscript



This is an *Accepted Manuscript*, which has been through the Royal Society of Chemistry peer review process and has been accepted for publication.

Accepted Manuscripts are published online shortly after acceptance, before technical editing, formatting and proof reading. Using this free service, authors can make their results available to the community, in citable form, before we publish the edited article. We will replace this *Accepted Manuscript* with the edited and formatted *Advance Article* as soon as it is available.

You can find more information about *Accepted Manuscripts* in the [Information for Authors](#).

Please note that technical editing may introduce minor changes to the text and/or graphics, which may alter content. The journal's standard [Terms & Conditions](#) and the [Ethical guidelines](#) still apply. In no event shall the Royal Society of Chemistry be held responsible for any errors or omissions in this *Accepted Manuscript* or any consequences arising from the use of any information it contains.

Cite this: DOI: 10.1039/c0xx00000x

www.rsc.org/xxxxxx

ARTICLE TYPE

Ce-/S-Codoped TiO₂/Sulfonated Graphene for Photocatalytic Degradation of Organic Dyes

Yingying Fan,^{a,b} Dongxue Han^{a*}, Bin Cai,^{a,b} Weiguang Ma,^{a,b} Mohsin Javed,^{a,c} Shiyu Gan,^{a,b} Tongshun Wu,^{a,b} M, Siddiq,^c Xiandui Dong^{a*}, Li Niu^a

⁵ Received (in XXX, XXX) Xth XXXXXXXXX 20XX, Accepted Xth XXXXXXXXX 20XX
DOI: 10.1039/b000000x

TiO₂ as an abundant and environmentally benign material equips a wide band gap which greatly confines its applications in photocatalysis. Doping and material-composition are both generally used to change and control the photocatalytic activity of semiconductors. Herein, we firstly propose a physical assembling method to deposit Ce-/S- codoped TiO₂ nanoparticles (NPs) on water-soluble sulfonated graphene (SGE) sheets, which guarantees a direct contact and satisfactory electron transfer between semiconductor and graphene. The Ce/S-TiO₂ NPs are homogeneously fixed on the surface of SGE sheets with the average particle size of ~ 7 nm. The resulted composite showed a noticeable photocatalytic activity in photodegradation of methyl orange ($\kappa = 0.425 \text{ h}^{-1}$). This promoted performance can be attributed to the synergistic effects of Ce- and S- codoping toward TiO₂ and the composite action between TiO₂ NPs and SGE. This kind of novel composite are expected to stimulate the development of doped and graphene-involved photocatalysts for addressing environmental problems.

1. Introduction

TiO₂ is regarded as one of the most promising photocatalyst materials due to its high photostability, nontoxicity, and economical availability. Nevertheless, the large band gap (3.0 ~ 3.2 eV) of TiO₂ makes it only active in UV irradiation which just accounts for 4% in the natural sunlight.¹⁻⁷ Concerning on this, doping methods have been widely applied to promote its photocatalytic performance towards visible light region.⁸⁻¹¹ Among that, metal doping could suppress the recombination of photogenerated electrons and holes since the doped metal ions always act as the electron traps, while non-metal doping could reduce the band gap to make TiO₂ active in visible light through modulating the energy band.¹²⁻¹⁵ Cerium, a kind of metal dopant, can not only give rise to enhancing optical properties due to its redox pair (Ce³⁺/Ce⁴⁺) but inhibiting the crystal growth of TiO₂ through the formation of Ce-O-Ti chemical bonds.^{9, 16} While Sulfur has been known as one of the most preferred non-metal dopant due to its multiple oxidation states located in bulk TiO₂.^{14, 17} Thus the combination of metal and non-metal doping might be expected to process a synergistic effect in greatly promoting the properties of TiO₂. Owing to its unique structure and properties, graphene has been widely investigated and has shown great potential in the synthesis of composite nanomaterials.^{18, 19} So far, despite various strategies have been used to design the graphene-based semiconductor photocatalysts,^{17, 18, 20-24} directly anchoring the synthesized nanoparticles (NPs) on graphene sheets was seldom

reported. The key reason is that NPs and graphene should possess adequate surface-active-sites for effective contact between each other, and the binding force should be equipped to make NPs adhere to the graphene plane firmly enough.^{19, 25, 26} Whereas, the high van der Waals energy is willing to make the graphene prone aggregating, which hampers the contact between graphene and NPs.^{19, 25, 27, 28} Sulfonated graphene (SGE) is a kind of modified graphene with plenty of p-phenyl-SO₃H groups on graphene sheet surface as well as the edge. SGE not only equips with the high water-solubility but also has excellent charge conductivity.²⁹⁻³² Hence, the SGE shows great potentiality to support NPs on the basis of preserving the superiority of graphene. In the limited reports, some graphene based composite through certain functionalized groups have been synthesized, where these functionalized molecules served as the bridge between graphene and NPs.^{18, 33} However, due to the indirect contact between NPs and graphene, the transport of the photo-induced carriers from the semiconductor NPs to graphene is significantly limited. Electrostatic interaction as a combining treatment might be worth considering in the composition synthesis.³⁴

In this work, Ce-/S-codoped TiO₂ NPs were prepared via a sol-gel method and then deposited directly on SGE nanosheets by means of electrostatic attraction. The Ce/S-TiO₂ NPs were found to distribute homogeneously on the surface of the SGE sheets and their average size is ~ 7 nm. The resulted nanocomposite (Ce/S-TiO₂/SGE) showed enhanced photocatalytic activity ($\kappa = 0.425 \text{ h}^{-1}$) than Ce- and S- single-doped or codoped TiO₂ composite in degradation of methyl orange (MO). This promoted performance

should be attributed to the synergistic effects of Ce- and S-codoping toward TiO₂ and the unique properties of SGE. A possible mechanism for photocatalytic behaviour of Ce/S-TiO₂/SGE system was also proposed.

2. Experimental

2.1 Chemicals

All chemical reagents applied in experiments were AR grade and used as received without further purification. Cerium nitrate hexahydrate was obtained from Aladdin industrial Corporations using as cerium precursor. Titanium (IV) butoxide (TBOT) was purchased from Sigma-Aldrich. Thiourea and ethanol were used as sulfur precursor and solvent, respectively. They were both purchased from Beijing Chemical Factory (Beijing, China). Graphite powder (99.9 %, 325 mesh) and sodium borohydride (NaBH₄) were also obtained from Beijing Chemical Factory (Beijing, China). Deionized water was used as aqueous solution with a resistivity of 18.2 MΩ cm.

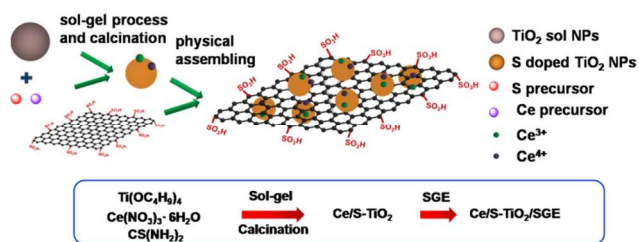
2.2 Synthesis of Ce/S-TiO₂/SGE nanocomposites

The Ce/S-TiO₂ nanoparticles were synthesized by sol-gel method which was been reported particularly suitable to achieve the homogeneous incorporation of dopants and the formation of ultrafine and uniform NPs.³⁵⁻³⁷ During the sol-gel process, the dopant precursors are inclined to be wrapped by polymeric Ti-O-Ti chains formed from the hydrolysis of TBOT, which finally lead to the uniform distribution of the dopants. And the synthetic process is simply depicted in Scheme 1.

Typically, 15.65 mg thiourea (as sulfur precursor) and 19.14 mg Cerium nitrate hexahydrate (as cerium precursor) were dissolved in 900 mL deionized water and the pH was adjusted to 2.0 with nitric acid. Then to this mixture, 100 mL ethanol solution of TBOT ($V_{\text{ethanol}} / V_{\text{TBOT}} = 95 / 5$) was injected slowly with vigorous stirring. The reaction system was kept stirring for 4 h to complete the hydrolysis of TBOT and then the dispersion was dried at 100 °C for 24 h. Afterwards, the sample was calcined at 500 °C for 1 h with a heating rate of 3 °C min⁻¹ to achieve preferable crystallization and remove the impurities. Meanwhile, it is known that the higher the crystallinity is, the fewer bulk defects exit, and the better photocatalytic performance achieved. The SGE was synthesized with similar procedure described by Yongchao Si and Guixia Zhao.³⁸ For preparation of Ce/S-TiO₂/SGE, 2 mg SGE was added to a mixture of 20 mL deionized water and 10 mL ethanol by mild sonication for 2 min. Then, 0.2 g Ce/S-TiO₂ was added to the suspension with constant sonication for 5 min and then stirring for 30 min. After rinsing with water for several times, the final production was dried at room temperature. The Ce-doped TiO₂ and S-doped TiO₂ was prepared by using individual Cerium nitrate hexahydrate or thiourea as doping agent and the pristine TiO₂ without doping agents.

2.3 Characterization

X-ray diffraction (XRD) measurements were carried out by a D8 Focus diffractometer (Bruker) with Cu Kα radiation ($\lambda = 0.15405$ nm). The Scherrer equation $D = K \lambda / \beta \cos \theta$, is applied to estimated the NPs size, in which D represents the crystallite size, K is the coefficient 0.89, λ is the wavelength of X-ray, β is



Scheme 1. Illustration of the formation of Ce/S-TiO₂/SGE.

the half-height width of the diffraction [101] peak of anatase and θ is the diffraction angle. High-resolution transmission electron microscopy (HRTEM), element mapping images were performed on a Hitachi-600 TEM with an accelerating voltage of 100 kV. The X-Ray photoelectron spectroscopy (XPS) analysis was obtained with an ESCALAB MKII X-ray photoelectron spectrometer using monochromated Al Kα X-rays. Ultraviolet visible (UV-Vis) absorption and UV-Vis diffuse reflectance spectra (using BaSO₄ as the reference) were taken using a Hitachi U-3900 spectrometer. Raman spectra were obtained on a Renishaw Raman system model 2000 spectrometer using a 514.5 nm argon ion laser and calibrating referenced to the 520 cm⁻¹ line of silicon. Fourier transform infrared spectra (FTIR) were collected on a Bruker Tensor 27 spectrometer. Zeta potential measurements were performed using a Zetasizer NanoZS (Malven Instruments).

2.4 Evaluation of photocatalytic activity

The photocatalytic activity was evaluated by photodegradation of methyl orange (MO) with the photocatalyst (50 mg) suspended in MO solution (50 mL, 10 mg L⁻¹) basing on the absorption spectroscopic technique. To obtain the adsorption equilibrium, the mixture was kept stirring in the dark for 30 min before degradation reaction. The photoreaction light source was a 500 W xenon arc lamp (CHF-XM35-500w, Beijing Trusttech Co. Ltd, China) equipped with a UV cut off filter ($\lambda > 420$ nm). At given time intervals, a specified volume dispersions (1 mL) were pipetted and then analyzed by recording variations of the absorption band maximum (463 nm) in the visible spectra of MO.

3. Results and Discussion

3.1 Morphology and chemical composition

XRD patterns were revealed in Fig. S1 to confirm the crystallographic phase of the samples. As shown in Fig. S1a, the XRD patterns of S-TiO₂, Ce/S-TiO₂ and Ce/S-TiO₂/SGE samples display distinct peaks (2θ) at 25.7°, 37.8°, 48.1°, 53.9° and 62.85°, which represent the anatase crystal planes of [101], [004], [200], [105] and [204] of TiO₂, respectively.^{1, 19, 26} According to Scherrer equation $D = K \lambda / \beta \cos \theta$, the crystalline sizes of S-TiO₂, Ce/S-TiO₂ and Ce/S-TiO₂/SGE are calculated as ~ 14, 7 and 7 nm. It is indicated that the participation of Ce played a vital role in preventing the growth of the NPs.^{39, 40} From Fig S1b, broader peaks of Ce-TiO₂ can be discovered in comparison with pristine TiO₂, which was due to the smaller sizes of Ce-TiO₂ and further confirm the action of Ce. Moreover, there are hardly distinctions between the XRD curves of Ce/S-TiO₂ and Ce/S-TiO₂/SGE, which indicated that the physically introduced SGE

has no impact on the structure of NPs.

Zeta potential was measured to prove the intimate contact between Ce/S-TiO₂ NPs and SGE. Probably owing to the existence of Ce³⁺/Ce⁴⁺ on the surface of NPs, the Ce/S-TiO₂ NPs (Zeta potential (ZP) = 11.6 mV) demonstrated positive charge, while the SGE with *p*-phenyl-SO₃H exhibit a negative property (ZP = -30.3 mV). Thus, an electrostatic interaction could be achieved and promote the dispersion of Ce/S-TiO₂ NPs on SGE.

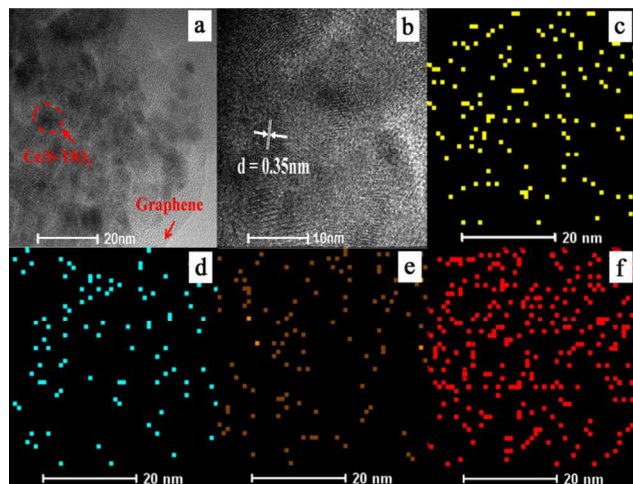


Fig. 1 (a) Typical TEM of Ce/S-TiO₂/SGE photocatalyst. (b) High-resolution TEM image. (c-h) Element Mapping Analysis of Ce/S-TiO₂/SGE, Ti (c), Ce (d), S (e), C (f).

In order to investigate the homogenous distribution of Ce/S-TiO₂ NPs on the surface of SGE, typical HRTEM image and element mapping of Ce/S-TiO₂/SGE were performed. As shown in Fig. 1a, the Ce/S-TiO₂ NPs with an average size of ~ 7 nm are deposited homogeneously on the surface of SGE, which is well agreed with the calculation results of XRD analysis. This demonstrated that by applying such a direct physical assembling approach, the perfect combination of SGE and Ce/S-TiO₂ NPs can be successfully acquired through electrostatic bonding, which is also theoretically accordance with the zeta potential measurements. Fig. 1b shows a well-defined crystalline lattice which can be identified with a *d* spacing of 0.35 nm matching the [101] plane of anatase TiO₂ (JCPDS card no. 04-0477). The elemental mappings of the above-mentioned Ce/S-TiO₂/SGE sample are showed in Fig. 1c, d, e, f, which reveal the uniform element distributions of Ce (d), S (e), Ti (c) and C (f). The homogeneous distribution of all above elements indicates that Ce and S are well distributed within the Ce/S-TiO₂ NPs while Ce/S-TiO₂ NPs are also well attached to SGE. The above-mentioned morphology is in good line with the proposed structure of Ce/S-TiO₂/SGE shown in Scheme 1.

It is well-known that the characteristics of carbon materials in Raman spectra are the D band (~1353 cm⁻¹) and the G band (1603 cm⁻¹), which relates to the sp³ carbon atoms vibrations of defects and E_{2g} phonon of sp² bonds of carbon atoms, respectively. The intensity ratio of the two bands (*I*_D / *I*_G) can reflect the defects and disorders of the graphitized structures.^{38, 41, 42, 43} From Fig. 2a, it is found that the ratios (*I*_D / *I*_G) of SGE and Ce/S-TiO₂/SGE are 0.98 and 1.00, respectively, which revealed that no defects and disorders were introduced during the physical mixing of SGE and Ce/S-TiO₂ NPs in the formation of the Ce/S-TiO₂/SGE hybrid.⁴⁴

Nevertheless, the typical D-band and G-band at ca. 1353.2 and 1599.1 cm⁻¹ moves to a lower frequency at ca. 1345.9 and 1599.1 cm⁻¹, which confirmed the mutual effect between Ce/S-TiO₂ and SGE. Meanwhile, Fig. 2b displays three main bands in the spectra at ca. 392.7, 513.4 and 634.4 cm⁻¹, which are assigned to A_{1g}, B_{2g} and E_g of the anatase TiO₂, respectively.

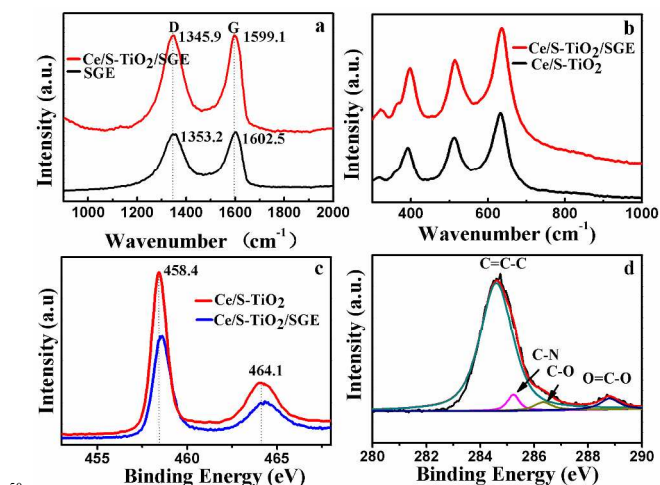


Fig. 2 (a) Raman spectra of SGE and Ce/S-TiO₂/SGE in range from 900-2000 cm⁻¹; (b) Raman spectra of Ce/S-TiO₂ and Ce/S-TiO₂/SGE in range from 300-1000 cm⁻¹; (c) XPS spectra of Ti 2p of Ce/S-TiO₂, Ce/S-TiO₂/SGE; (d) XPS spectra of C 1s of Ce/S-TiO₂/SGE.

The surface chemical compositions and chemical states of Ce/S-TiO₂/SGE, Ce/S-TiO₂ are investigated from their XPS spectra (shown in Fig. 2c, d and S2a, b). The XPS spectrum of the Ti species (Fig. 2c) displays two bands at ca. 458.4 and 464.1 eV, which can be attributed to Ti 2p_{3/2} and 2p_{1/2} binding energies with a spin-orbital doublet splitting of 5.7 eV (Δ) (Ti 2p_{1/2}-Ti 2p_{3/2}) in line with the 4+ oxidation state of titanium.^{39, 45, 46, 47} The Ti 2p binding energy of the Ce/S-TiO₂/SGE sample increases as compared to that of Ce/S-TiO₂, which is because Ce/S-TiO₂ NPs serve as electron donors and SGE facilitates the charge transfer, and the CB electrons of Ce/S-TiO₂ may transfer to the SGE. And thus resulted in a decrease in the outer electron cloudy density of Ti ions.⁴¹ Fig. S2a reveals that a distinct peak at 168.5 eV that represents the S⁶⁺ exists in the Ce/S-TiO₂. And the existential state of S⁶⁺ in Ce/S-TiO₂ crystal lattice is mainly acting as the substitution of Ti⁴⁺.^{17, 39, 48} From the comparison of Ce/S-TiO₂ and Ce/S-TiO₂/SGE, a much broader peak was observed as the introduction of SGE, which can be ascribed to the S⁴⁺ in the *p*-phenyl-SO₃H. The spectrum (Fig. S2b) of Ce encounters little change from Ce/S-TiO₂ to Ce/S-TiO₂/SGE. As shown in Fig. 2d, the C 1s XPS of Ce/S-TiO₂/SGE demonstrated four types of carbon which are observed as C=C-C (284.6 eV), C-N (285.2 eV), C-O (286.3 eV) and O=C-O (288.8 eV). The low intensities of the oxygen functional groups further confirmed the reduction of GO and the peak of C=C-C indicates the intact existence of the graphitized conjugated sp² carbon network.^{44, 49, 50} Meanwhile the presence of C-N at 285.2 eV manifests the existence of diazonium *p*-phenyl-SO₃H groups which ensures the water solubility of SGE.^{29, 38} And the presence of the SGE in the composite of Ce/S-TiO₂/SGE is also testified by FTIR spectra shown in supporting information (Fig. S3).

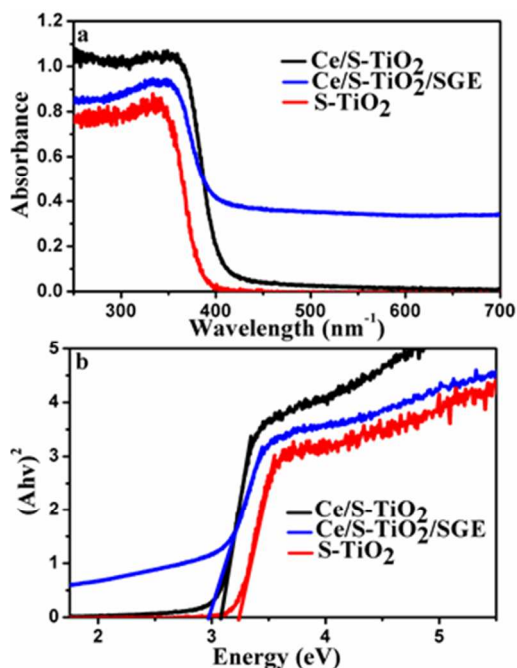


Fig. 3 (a) UV-Vis diffuse reflectance spectra of S-TiO₂, Ce/S-TiO₂ and Ce/S-TiO₂/SGE. (b) Plot of transformed Kubelka-Munk function *versus* the energy of light.

3.2 Optical property and photocatalytic performance

It is well known that the absorption range of light plays a significant role towards the photocatalytic activity of semiconductor catalysts. Fig. 3a and S4 illustrates the UV-Vis diffuse reflectance spectra of the preformed S-TiO₂, Ce/S-TiO₂, Ce/S-TiO₂/SGE, TiO₂ and Ce-TiO₂ samples. As shown in the curve of Ce/S-TiO₂/SGE (blue line), a red shift occurred compared to Ce/S-TiO₂ as the incorporation of SGE, which suggested a narrower band gap of the Ce/S-TiO₂/SGE. It is also observed a strong visible light absorption of Ce/S-TiO₂/SGE sample in the range from 417 nm to 700 nm as compared with the sample of Ce/S-TiO₂ since SGE is a good visible light absorber,³² which can greatly improve the absorbance. A plot of the transformed Kubelka-Munk function (Fig. 3b) revealed that the energy gaps of S-TiO₂, Ce/S-TiO₂ and Ce/S-TiO₂/SGE are 3.18, 3.07 and 2.95 eV, respectively. These results also support the qualitative observation of the red shift described in Fig. 3a.

As always, photodegradation of organic dyes is used to investigate the photocatalytic activity. Here, the photocatalytic degradation of 10 mg L⁻¹ MO was utilized to verify the enhanced photocatalytic performance of the semiconductor-graphene nanocomposites Ce/S-TiO₂/SGE. The degradation experiment was performed under irradiation in the visible light ($\lambda > 420$ nm), and the degradation results are shown in Fig. 3a. In accordance with the Lambert-Beer law, the real-time concentration variations (C/C_0) of MO during the photodegradation are in direct proportion to the normalized maximum absorption values (A/A_0) (Fig. S6).⁵¹⁻⁵² C and C_0 refer to the concentration of MO at real time t and at 10 mg L⁻¹, respectively.

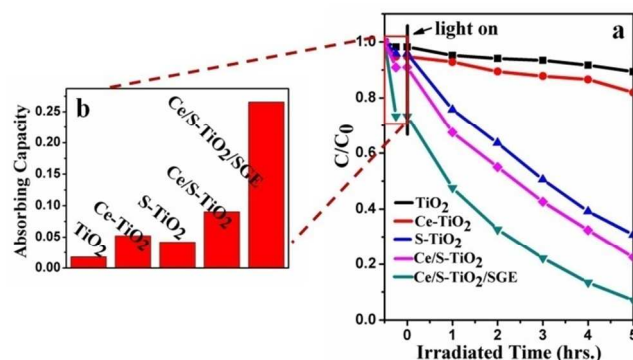


Fig. 4 (a) Photodegradation dynamic curves of MO over TiO₂, S-TiO₂, Ce/S-TiO₂ and Ce/S-TiO₂/SGE. (b) Bar plot shows the adsorbing capacity of TiO₂, Ce-TiO₂, S-TiO₂, Ce/S-TiO₂, Ce/S-TiO₂/SGE samples after reaching the adsorption equilibrium in the dark for 30 min.

Pristine TiO₂, Ce-TiO₂, S-TiO₂ and Ce/S-TiO₂ were served as the standard photocatalysts in the control experiments, respectively. The adsorptive capacity of the samples has been measured after keeping the degradation system in the dark for 0.5 h to obtain adsorption equilibrium before the photocatalytic test (Fig. 4b). Fig. 4a displays that contrasted with pristine TiO₂, S-TiO₂ and Ce-TiO₂, Ce/S-TiO₂ has a promoted photocatalytic ability when, which should be attributed to the synergistic effect of Ce and S. As S doped, the S 3p would mix with the valence band of TiO₂ and thus resulting in narrowing the band gap, which leads to the easy separation of photo-induced charges.^{37, 53} Meanwhile, the Ce⁴⁺/Ce³⁺ pair acting as the electron scavenger could further promote the segregation of electrons and holes. The Ce-O-Ti at the crystal surface can efficiently control the growing of the crystal and helps to maintain a relatively large specific area of the NPs.^{39, 54} Due to the synergistic effects of Ce/S-TiO₂ and SGE, Ce/S-TiO₂/SGE ($\kappa = 0.425$ h⁻¹) obtains an ascension in photodegradation ability compared to Ce/S-TiO₂ ($\kappa = 0.259$ h⁻¹). The greater photocatalytic activity of Ce/S-TiO₂/SGE hybrid compared to Ce/S-TiO₂ NPs is mainly attributed to the three factors.^{37, 41} (i) the better utilization of solar energy: as described above, the introduction of SGE helped the photocatalyst absorb more visible-light, which meant that more photon energy would be used to excite the electrons from the valence band to the conduction band. (ii) the high-efficiency photo-induced charge carriers separation and transport: due to the high mobility of the electrons in the central portion of SGE sheets, the injected electrons can easily move throughout the vast majority of SGE sheet, thus efficiently decreases the recombination probability of the photoexcited electron-hole pair and leave more charge carriers to form the reactive sites. (iii) the excellent adsorption capacity of Ce/S-TiO₂/SGE due to its unique structure for dye molecules: the adsorption of MO upon Ce/S-TiO₂/SGE is not merely the simple physical adsorption, but also through the π - π conjugation between SGE and MO molecules, who has two benzene rings in the molecule structure. As a result, an obvious enhancement adsorption of MO achieved upon Ce/S-TiO₂/SGE compared with other photocatalysts (shown in Fig. 4b). Such an outstanding adsorption of MO molecules upon the surface of the photocatalyst could for granted facilitate the degradation of dye molecules. However, the adsorption tended to saturate within ~15 min with the adsorption capacity of about 25% without further

increasing (shown in Fig. S5). In order to investigate the error which should be brought by the adsorption capacity of photocatalyst, a higher initial concentration (double concentration) of MO was applied to evaluate the degradation ability of Ce/S-TiO₂/SGE (Fig. S7). It is observed that in the higher concentration of MO, with constant photocatalyst, the adsorption capacities of Ce/S-TiO₂ and Ce/S-TiO₂/SGE without light are 3.7% and 12.2% respectively, which seem much lower than those of under lower MO concentration. However, the overall degradation tendency mainly maintains no change. In addition, six successive photodegradation experiments have been carried out so as to evaluate the stability of Ce/S-TiO₂/SGE (Fig. S8). For the first three cycles, there seemed some decline in the degradation performance, which might be attribute to the mass loss of the photocatalytic hybrid with loose interactions during the circulation process. And in the next following three cycles, the photocatalyst tended to keep stable. The considerable stability further confirms the reproducibility and recycling of such Ce/S-TiO₂/SGE photocatalyst.

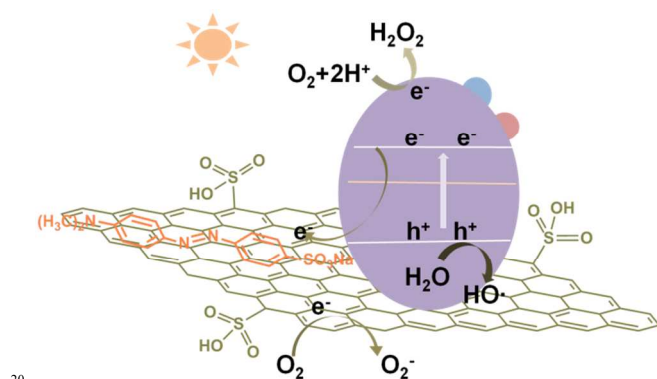


Fig. 5 Schematic illustration of photocatalytic enhancement mechanism of Ce/S-TiO₂/SGE.

A possible mechanism has been proposed to better understand the photocatalytic process of Ce/S-TiO₂/SGE (Fig. 5). When light illuminates on TiO₂ NPs, the impinging photons possessing equal or higher energies than the band gap energy of TiO₂ will excite the electrons from valence band to conduction band, which results in the generation of excited electrons in the conduction band and positive holes in the valence band. S dopant leads to the narrowing of band gap, so it becomes easier to separate the photo-induced charges under the same energy.^{14, 48} SGE who serves as both the electron acceptor and donor will succeed suppressing the charge recombination and making more reactive species to promote the degradation of MO. As the analysis in the previous research,^{41, 55-57} the separated electrons and holes play key roles in bringing forth the radicals and the activated oxygen species in the photocatalytic system, which are the considerable elements in decomposing the organic molecules. In our system, according to the same principle and relevant literatures^{35, 37, 39}, the following radicals and activated oxygen species might be achieved: $O_2 + e^- \rightarrow O_2^-$, $h^+ + H_2O \rightarrow HO\cdot + H^+$, $O_2 + 2H^+ + 2e^- \rightarrow H_2O_2$.^{37, 39, 41} Ce⁴⁺/Ce³⁺ pair on the surface of photocatalyst, who acts as an electron scavenger, will transmit electrons to the oxygen for production of O₂⁻.³⁹ Due to the collaborative effects of S, Ce codoping and the promotion of the adsorptive capacity of SGE as well as the inherent advantages of electron transmission

of graphene material, the photocatalytic ability of Ce/S-TiO₂/SGE has been obviously augmented.

4. Conclusion

In summary, a high performed visible-light-driven photocatalyst Ce/S-TiO₂/SGE has been synthesized depending on the combination of synergistic effects of Ce-/S- codoping and the incorporation of SGE. A series of effective and reliable characterizations have been applied to confirm the morphologies and physical structures of the Ce/S-TiO₂/SGE hybrid. The photocatalytic activity was evaluated by an introduced classic MO photodegradation model. Subsequently, a photocatalytic enhancement mechanism has been proposed to give an illustration for better understanding the photocatalytic process, which would stimulate the development of doped and graphene-involved photocatalysts for addressing environmental problems.

Acknowledgements

The authors are most grateful to the NSFC, China (No. 21205112, No.21225524 and No.21127006) and the Department of Science and Techniques of Jilin Province (No.20120308 and No.201215091) for their financial support.

Notes

^a State Key Laboratory of Electroanalytical Chemistry, c/o Engineering Laboratory for Modern Analytical Techniques, Changchun Institute of applied Chemistry, Chinese Academy of Science, Changchun, 130022, Jilin, China, Fax: +8643185262800; Tel: +8643185262425; E-mail: dxhan@ciac.ac.cn, dxj@ciac.ac.cn

^b University of Chinese Academy of Sciences, Beijing 100039, China
^c Department of Chemistry, Quaid-I-Azam University Islamabad, Pakistan

References

- N. Yang, Y. Liu, H. Wen, Z. Tang, H. Zhao, Y. Li and D. Wang, *ACS Nano*, 2013, **7**, 1504-1512.
- L.-W. Zhang, H.-B. Fu and Y.-F. Zhu, *Adv Funct Mater*, 2008, **18**, 2180-2189.
- J. B. Joo, M. Dahl, N. Li, F. Zaera and Y. Yin, *Energ Environ Sci*, 2013, **6**, 2082-2092.
- P. D. Cozzoli, R. Comparelli, E. Fanizza, M. L. Curri, A. Agostiano and D. Laub, *J Am Chem Soc*, 2004, **126**, 3868-3879.
- J. Tang, J. R. Durrant and D. R. Klug, *J Am Chem Soc*, 2008, **130**, 13885-13891.
- W. Li, F. Wang, S. Feng, J. Wang, Z. Sun, B. Li, Y. Li, J. Yang, A. A. Elzatahry, Y. Xia and D. Zhao, *J Am Chem Soc*, 2013, **135**, 18300-18303.
- W. Guo, F. Zhang, C. Lin and Z. L. Wang, *Advanced Materials*, 2012, **24**, 4761-4764.
- M. Gleń and B. Grzmil, *Chem. Pap.*, 2013, **67**, 1386-1395.
- T. Tong, J. Zhang, B. Tian, F. Chen, D. He and M. Anpo, *J Colloid Interf Sci*, 2007, **315**, 382-388.
- T. Tachikawa, S. Tojo, K. Kawai, M. Endo, M. Fujitsuka, T. Ohno, K. Nishijima, Z. Miyamoto and T. Majima, *The Journal of Physical Chemistry B*, 2004, **108**, 19299-19306.
- Y. Shu, H. Sun, X. Quan and S. Chen, *The Journal of Physical Chemistry C*, 2012, **116**, 25319-25327.
- F. B. Li, X. Z. Li, M. F. Hou, K. W. Cheah and W. C. H. Choy, *Applied Catalysis A: General*, 2005, **285**, 181-189.
- A. Charanpahari, S. S. Umare and R. Sasikala, *Appl Surf Sci*, 2013, **282**, 408-414.
- P. Xu, T. Xu, J. Lu, S. Gao, N. S. Hosmane, B. Huang, Y. Dai

- and Y. Wang, *Energ Environ Sci*, 2010, **3**, 1128-1134.
15. S. Hoang, S. P. Berglund, N. T. Hahn, A. J. Bard and C. B. Mullins, *J Am Chem Soc*, 2012, **134**, 3659-3662.
16. G. Xiao, X. Huang, X. Liao and B. Shi, *The Journal of Physical Chemistry C*, 2013, **117**, 9739-9746.
17. T. Ohno, M. Akiyoshi, T. Umebayashi, K. Asai, T. Mitsui and M. Matsumura, *Applied Catalysis A: General*, 2004, **265**, 115-121.
18. D. Wang, D. Choi, J. Li, Z. Yang, Z. Nie, R. Kou, D. Hu, C. Wang, L. V. Saraf, J. Zhang, I. A. Aksay and J. Liu, *ACS Nano*, 2009, **3**, 907-914.
19. Y. Zhang, Z.-R. Tang, X. Fu and Y.-J. Xu, *ACS Nano*, 2010, **4**, 7303-7314.
20. H. Zhang, X. Lv, Y. Li, Y. Wang and J. Li, *ACS Nano*, 2009, **4**, 380-386.
21. W. Yue, S. Jiang, W. Huang, Z. Gao, J. Li, Y. Ren, X. Zhao and X. Yang, *Journal of Materials Chemistry A*, 2013, **1**, 6928-6933.
22. O. Akhavan, M. Abdollahad, A. Esfandiar and M. Mohatashamifar, *The Journal of Physical Chemistry C*, 2010, **114**, 12955-12959.
23. J. E. Johns, J. M. P. Alaboson, S. Patwardhan, C. R. Ryder, G. C. Schatz and M. C. Hersam, *J Am Chem Soc*, 2013.
24. J. E. Johns, J. M. P. Alaboson, S. Patwardhan, C. R. Ryder, G. C. Schatz and M. C. Hersam, *J Am Chem Soc*, 2013, **135**, 18121-18125.
25. G. Williams, B. Seger and P. V. Kamat, *ACS Nano*, 2008, **2**, 1487-1491.
26. H. Zhang, P. Xu, G. Du, Z. Chen, K. Oh, D. Pan and Z. Jiao, *Nano Res.*, 2011, **4**, 274-283.
27. Q. Xiang, J. Yu and M. Jaroniec, *Chemical Society Reviews*, 2012, **41**, 782-796.
28. D. Du, J. Liu, X. Zhang, X. Cui and Y. Lin, *Journal of Materials Chemistry*, 2011, **21**, 8032-8037.
29. G. Zhao, L. Jiang, Y. He, J. Li, H. Dong, X. Wang and W. Hu, *Advanced Materials*, 2011, **23**, 3959-3963.
30. E. Coşkun, E. A. Zaragoza-Contreras and H. J. Salavagione, *Carbon*, 2012, **50**, 2235-2243.
31. L. Wang, D. Wang, S. Zhang and H. Tian, *Catalysis Science & Technology*, 2013, **3**, 1194-1197.
32. J. Ji, G. Zhang, H. Chen, S. Wang, G. Zhang, F. Zhang and X. Fan, *Chemical Science*, 2011, **2**, 484-487.
33. J. S. Lee, K. H. You and C. B. Park, *Advanced Materials*, 2012, **24**, 1084-1088.
34. H. Li, S. Gan, D. Han, W. Ma, B. Cai, W. Zhang, Q. Zhang and L. Niu, *Journal of Materials Chemistry A*, 2014, **2**, 3461-3467.
35. E. Traversa, M. Di Vona, S. Licoccia, M. Sacerdoti, M. Carotta, L. Crema and G. Martinelli, *Journal of Sol-Gel Science and Technology*, 2001, **22**, 167-179.
36. W. Li, F. Wang, S. Feng, J. Wang, Z. Sun, B. Li, Y. Li, J. Yang, A. A. Elzatahry, Y. Xia and D. Zhao, *J Am Chem Soc*, 2013.
37. X. Chen and S. S. Mao, *Chemical Reviews*, 2007, **107**, 2891-2959.
38. Y. Si and E. T. Samulski, *Nano letters*, 2008, **8**, 1679-1682.
39. M. Nasir, Z. Xi, M. Xing, J. Zhang, F. Chen, B. Tian and S. Bagwasi, *The Journal of Physical Chemistry C*, 2013, **117**, 9520-9528.
40. N. Yan, Z. Zhu, J. Zhang, Z. Zhao and Q. Liu, *Materials Research Bulletin*, 2012, **47**, 1869-1873.
41. B. Cai, X. Lv, S. Gan, M. Zhou, W. Ma, T. Wu, F. Li, D. Han and L. Niu, *Nanoscale*, 2013, **5**, 1910-1916.
42. S. Stankovich, D. A. Dikin, G. H. B. Dommett, K. M. Kohlhaas, E. J. Zimney, E. A. Stach, R. D. Piner, S. T. Nguyen and R. S. Ruoff, *Nature*, 2006, **442**, 282-286.
43. W. Guo, C. Chen, M. Ye, M. Lv and C. Lin, *Nanoscale*, 2014, **6**, 3656-3663.
44. O. Akhavan, *ACS Nano*, 2010, **4**, 4174-4180.
45. C. Wang, D. Meng, J. Sun, J. Memon, Y. Huang and J. Geng, *Advanced Materials Interfaces*, 2014, 1300150.
46. X. Yang, J. Qin, Y. Li, R. Zhang and H. Tang, *Journal of Hazardous Materials*, 2013, **261**, 342-350.
47. X. Yang, J. Qin, Y. Jiang, R. Li, Y. Li and H. Tang, *RSC Advances*, 2014, **4**, 18627-18636.
48. L. K. Randeniya, A. B. Murphy and I. C. Plumb, *J Mater Sci*, 2008, **43**, 1389-1399.
49. C. Chen, W. Cai, M. Long, B. Zhou, Y. Wu, D. Wu and Y. Feng, *ACS Nano*, 2010, **4**, 6425-6432.
50. B. Qiu, M. Xing and J. Zhang, *Journal of the American Chemical Society*, 2014, **136**, 5852-5855.
51. M. Shalom, S. Inal, C. Fettkenhauer, D. Neher and M. Antonietti, *J Am Chem Soc*, 2013, **135**, 7118-7121.
52. L. Zhang, D. Jing, X. She, H. Liu, D. Yang, Y. Lu, J. Li, Z. Zheng and L. Guo, *Journal of Materials Chemistry A*, 2014, **2**, 2071-2078.
53. X. Chen and C. Burda, *J Am Chem Soc*, 2008, **130**, 5018-5019.
54. V. Štengl, S. Bakardjieva and N. Murafa, *Mater Chem Phys*, 2009, **114**, 217-226.
55. O. Akhavan, *Carbon*, 2011, **49**, 11-18.
56. Y. Wen, H. Ding and Y. Shan, *Nanoscale*, 2011, **3**, 4411-4417.
57. L. Zhang, D. Zhang, J. Zhang, S. Cai, C. Fang, L. Huang, H. Li, R. Gao and L. Shi, *Nanoscale*, 2013, **5**, 9821-9829.